Hindawi
Mobile Information Systems
Volume 2022, Article ID 9739770, 9 pages
https://doi.org/10.1155/2022/9739770

Research Article

Calculation and Function of Composition Proportion in Photography Based on Digital Information Technology

Guodong Feng

National Demonstration Center for Experimental Designing Art Education, Tai Yuan University of Technology, Jinzhong 030600, Shanxi, China

Correspondence should be addressed to Guodong Feng; fengguodong@tyut.edu.cn

Received 17 February 2022; Revised 22 April 2022; Accepted 30 May 2022; Published 22 June 2022

Academic Editor: Chia-Huei Wu

In order to take better pictures, a method of composition proportion in photography based on digital information technology is proposed. Feature extraction is carried out from the captured pictures, and the modular customized design of digital information technology is adopted. The research is carried out in the two fields of image blur and approximate repeated image de redundancy. An improved image blur algorithm based on bag of words (bag of words) kernel function is proposed. The experimental results show that the coarse matching time is the time spent in matching a query image with thousands of images in the database, and the fine matching time is the time spent in matching a query image with eight candidate images with orb. The total query time is about 0.7 seconds, while it takes about 500 seconds to match thousands of images only with orb algorithm. In general, we combine coarse matching and fine matching, which can balance the accuracy and speed well. It is proved that the digital information technology proposed in this paper has a good effect in the calculation and function of composition proportion in photography.

1. Introduction

At present, the research and practice of modular customized design using digital information technology are still in the development stage. In the research stage, modular customization design applies the design method of digital information technology, but the concept of module is not complete; the modular customized design in the practical stage still has development potential in form diversity and space quality. In recent years, with the vigorous development of information technology and Internet applications, multimedia massive data are growing at an unimaginable speed. As a common information carrier, digital image has an indispensable position [1]. With the popularity of social software such as microblog and WeChat and the popularity of intelligent camera, everyone can easily capture, process, and spread images, so the image data on the Internet are increasing in an unpredictable way. While digital image technology enriches our life, some problems are becoming increasingly prominent. Shooting angle refers to the angle presented by the relative position between the camera and the subject. In life, people observe things with their eyes at a certain angle. The choice of this angle usually represents some behavior habits and psychological characteristics of people. Therefore, the choice and change of shooting angle evolved from people's lives and habits. The choice of angle means the starting point of looking at things. The choice of angle can reflect the photographer's psychology and represent the photographer's position [2]. Angle has subjectivity and distinct personality. It can strengthen and highlight some things but also weaken and dilute the performance of some things. The choice of different angles has different emphases and expressiveness. In terms of photography art, the expression theme is different, and the angle selection is different. The composition has different ideas and different angles. The change of angle is complex and changeable. Shooting a thing or theme has countless shooting points to choose from in the three-dimensional space around it. Students need to learn, think, and master how to make rational use of these shooting points regularly and methodically and find out the best shooting angle. The complex changes of shooting angle can be divided into three

categories: changes in shooting direction, changes in shooting height, and changes in shooting distance. The angles in the shooting direction can be summarized as front, side, oblique side, and back. The angle of shooting height is flat shot, overhead shot, and overhead shot. The change of shooting distance is the change caused by changing the focal length of the lens or the object distance between the shooting point and the subject, that is, the five categories of long-range, panoramic, medium range, close-up, and close-up. These angles and scenes can be used singly, and there are also repeated and overlapping collocations, which reflect a strong complementary relationship [3]. Through the reasonable selection and application of these changes, we can better express the theme, more skillfully render the various relationships between people, characters, and the environment, and better help readers understand the intention of the picture. The choice of angle should be novel and unique. On the basis of logic, we should break the traditional viewing mode and find another way. Find unusual shooting angles from common scenes. The shooting angle is novel, and the content and form of expression are unique. Only in this way can we be unconventional and make the picture unconventional and refreshing to the viewer.

2. Literature Review

JM Davidson proposed two noise sensitivity estimation methods called different focus evaluation functions in the subsequent study of automatic focusing methods [4]. Of course, these two methods need to calculate all the focusing methods in the process of selecting the best focusing method. For some occasions with high real-time requirements, the application of this selection method is limited. Despite some limitations, this paper also makes many new attempts to quantitatively evaluate the auto focus function. In the study by Clero et al., according to the basic imaging principle of the imaging system, a defocus blur estimation method based on the point spread function is proposed on the basis of the point spread function, and the image restoration filtering technology is also applied to the automatic focusing system, and a better effect is obtained [5]. Reichardt et al. used the optical autocollimation method to develop the automatic focusing system for integrated circuit lithography [6]. Shavkat et al. used analog circuit to detect the high-frequency component in the circuit signal and apply it in the automatic focusing of camera [7]. In the study by Hong et al., the teaching and research office of optical instruments has developed the automatic focusing system in satellite photography equipment by using the autocollimation method [8]. Jin et al. studied the automatic focusing system of image detection band cutting differential comparison CCD. Shanghai Institute of laser technology has studied the automatic focusing technology of the microscopic system of optical disc recorder and player by using the astigmatism method [9]. Liang et al. studied the automatic focusing of the microscopic system of the linewidth measuring instrument by using the eccentric beam method and reached the international advanced level [10]. Song et al. used CCD camera technology and image processing method to automatically screen biological pictures [11]. Mark et al. and others mainly focus on the research of image gray gradient and put forward the sum of image gray gradient vector modulus square, Roberts gradient, and Laplace operator, as well as the autofocus evaluation function of digital image processing. Using the above three mathematical models of focus evaluation function, the experimental results of defocus blur and motion blur are given, compared, and analyzed. The following conclusions are obtained: these focus evaluation functions have the characteristics of good unbiased, unimodal, and high sensitivity and can be applied to the evaluation of defocus blur and motion blur, and the modulus sum of gray gradient vector is the most ideal focus evaluation function [12]. Dai et al. and others analyzed the application of gradient function, spectrum function, and entropy function in autofocusing technology, respectively, and studied and analyzed the performance of the evaluation function of autofocusing together. In the experiment, a large number of comparisons are made between the energy gradient function and the spectrum function, and it is concluded that the spectrum function is better than the energy gradient function in sensitivity. However, in terms of processing time, the processing time of energy gradient function is shorter than that of spectrum function, so the real-time performance of energy gradient function is better than that of spectrum function [13].

Based on the current research, this paper proposes a method of composition proportion in photography based on digital information technology. Feature extraction is carried out from the captured pictures, and the modular customized design of digital information technology is adopted. The research is carried out in the two fields of image blur and approximate repeated image de redundancy, and an improved image blur algorithm based on bag of words is proposed.

3. Image Blur Algorithm Based on Word Bag Model

Then, we use a novel feature point detection algorithm based on concentric rings to obtain the feature points. Next, we use the improved Gabor filter-based feature description algorithm to describe each feature point. After feature extraction of all images in the image database, all feature point descriptors of all images are clustered into a "visual dictionary" by the K-means algorithm. Finally, this "visual dictionary" is used to obtain the final "visual signature" of each image and save it for later matching (Figure 1).

Blurring stage of photographed image: as shown in Figure 2, when an image to be queried is obtained, we first extract feature points and obtain descriptors of each feature point using the same method mentioned in the database building stage. Then, use the "visual dictionary" saved in the database building stage to generate the "visual signature" of this figure. Then, the "visual signature" will be roughly matched with the "visual signature" of all images saved in the database to obtain a group of candidate similar images [14].

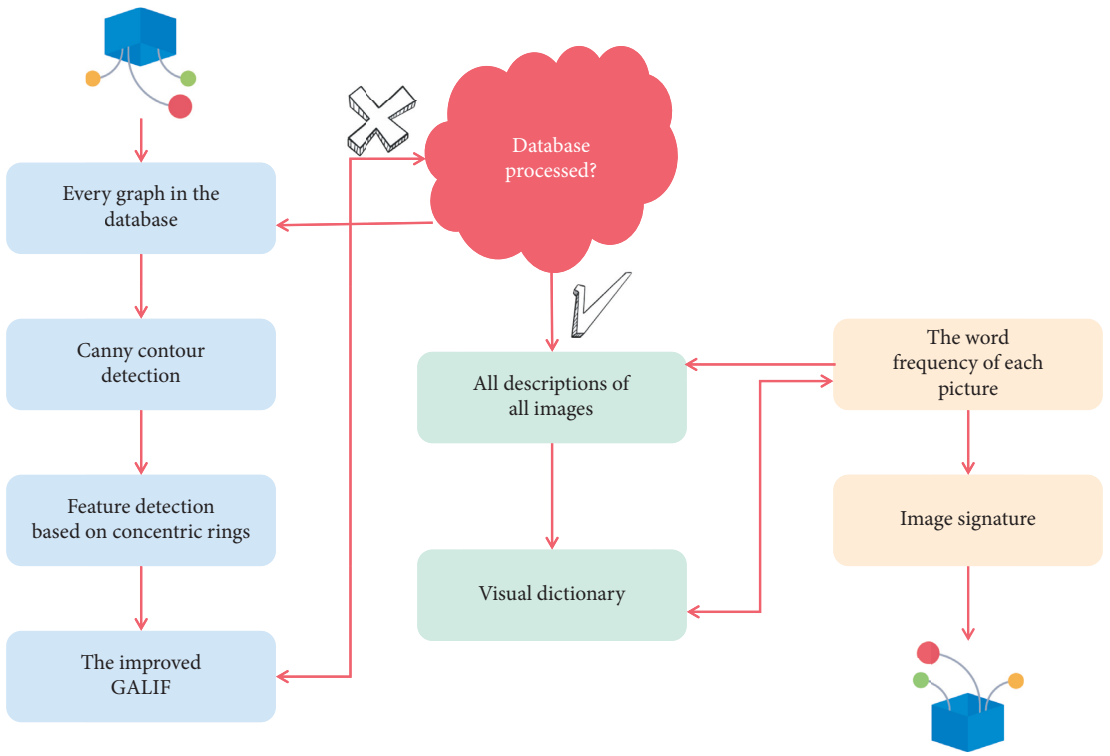

Figure 1: Image database construction stage.

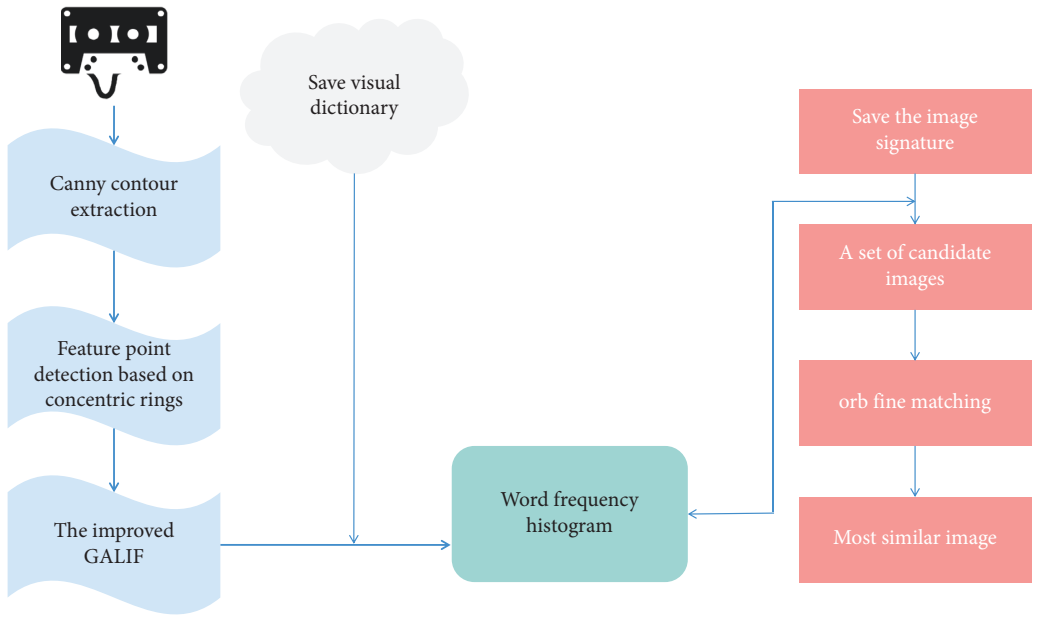

Figure 2: Blurring stage of photographic image.

3.1. Feature Point Detection Method Based on Concentric Ring. From the data in Table 1, it can be seen that although the number of detected feature points has changed, this transformation is small for the number of feature points of the whole image and can not be considered. Therefore, the feature point extraction algorithm based on concentric rings can resist image selection, noise, and scale transformation and has strong robustness.

3.2. Feature Point Description Method Based on Gabor Filter. In terms of computer vision, Gabor feature is very suitable for processing camera images and has the following advantages:

(1) Because Gabor kernel function filters the DC component of the filtered image, it can resist the transformation caused by local illumination and is very suitable for processing camera images.

Table 1: Different image attack experiments.

Rotation attack	Rotation angle	Original drawing	30°	60°	90°	135°
	Feature points	300	290	294	301	305
Noise attack	Noise type	Original drawing	Salt and pepper noise (strong)	Salt and pepper noise (weak)	Gaussian noise (strong)	Gaussian noise (weak)
	Feature points	300	311	305	314	302
Scale transformation	Ruler size	Original drawing	5 times smaller	3 times smaller	2 times smaller	4 times smaller
	Feature points	300	285	292	308	310

(2) Gabor filtering results can describe the gray distribution information of images in different scales and directions. Therefore, it can not only describe the global information in a large scale to reduce the impact of noise but also describe the local details in a small scale. Firstly, the object of Gabor filtering is the contour map, so it only filters the lines in the contour, and the local lines contain little useful information. Secondly, Gabor filters the image and then extracts local small blocks, which is very time-consuming; Finally, Gabor does not resist rotation transformation. In view of the above shortcomings, this paper improves the Gabor and applies the improved Gabor to the ambiguity of the image taken by the camera. The specific extraction process after the improvement is as follows:

(1) For each feature point p_i extracted by the feature point extraction algorithm based on concentric rings, calculate its local coordinate system, take the connecting direction between the center point o of the rectangular box and p_i as the ordinate, and take the straight line passing through p_i and perpendicular to the ordinate as the abscissa x_i. As shown in Figure 3, each feature point has its own local coordinate system.

(2) Draw a small block of N around Pi on the gray image corresponding to feature point P instead of the previous local line, as shown in Figure 3 [15].

(3) Because the region A_i may contain multiple pixels, we calculate that the average value of the filtering results of the region A_i in the o_j direction is a_{ij}. The average values of the filtering results of the four regions in the 8 directions together form the feature vector F, as shown in Figure 4.

The improved Gabor changes the filtering object from the original local line to the corresponding gray image, making full use of more information on the image. Due to the use of the local coordinate system, the improved Gabor can resist rotation transformation. At the same time, the filtering area does not filter the whole image but only the small blocks around the feature points, so the filtering time has been greatly improved. Table 2 shows the efficiency of changing the filtering area from the whole image to small patches around the feature points, D is the improved parameter above, and the parameter t is the ratio of the actual filtering area of the local patches around the filtering feature to the filtering area of the entire image; it can be seen from Table 2 that when the number of feature points is between 100 and 1000, the value of T is between 1% and 3%; that is, the actual filtering area only accounts for 1% to 3% of the overall image.

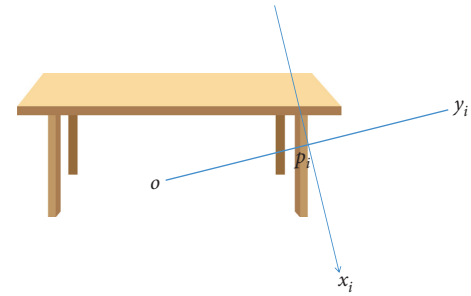

Figure 3: Local coordinate system of feature point P.

Figure 5 is a group of images rotated from the original image through various angles. We use the images to test the antirotation performance of our algorithm. We use our improved feature extraction based on the word bag model (including the improved Gabor algorithm) to extract a final descriptor from each image and then use the kernel regression nonuniform interpolation algorithm of structural tensor to calculate their fuzziness. Their differences are listed in Table 3. According to the data in the table, our algorithm can resist rotation.

3.3. Kernel Regression Nonuniform Interpolation Algorithm Based on Structural Tensor. Kernel regression is a nonparametric regression based on statistics. Consider the random variables X, y, hypothesis

$$y_i = m(x_i) + \varepsilon_i, i = 1, \ldots, n, \tag{1}$$

where

$$E(\varepsilon_i) = 0, D(\varepsilon_i) = \sigma^2 < \infty. \tag{2}$$

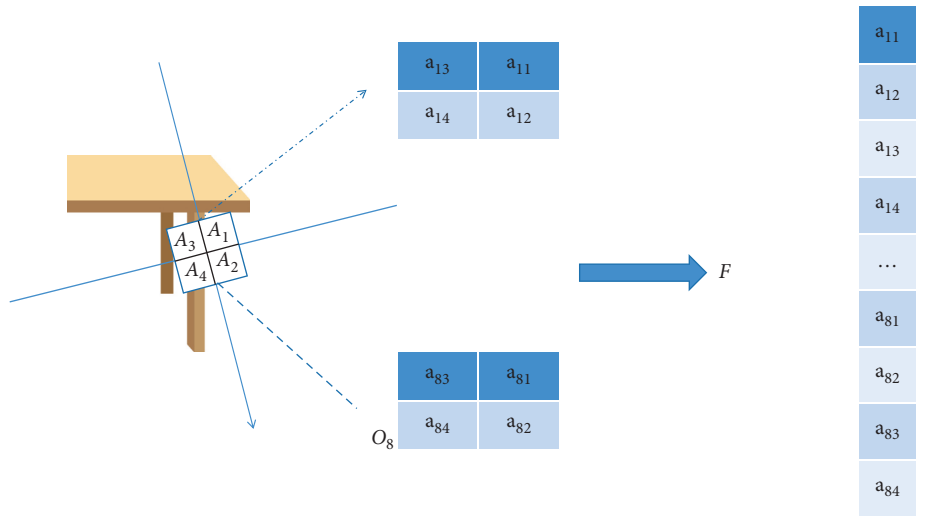

Figure 4: Improved Gabor extraction process.

Table 2: Efficiency of local block filtering.

Number of feature points	a	d	Small block size	T (%)
100	0.025	9	5 × 5	1
	0.05	18	9 × 9	3
1000	0.025	9	5 × 5	10
	0.05	18	9 × 9	30

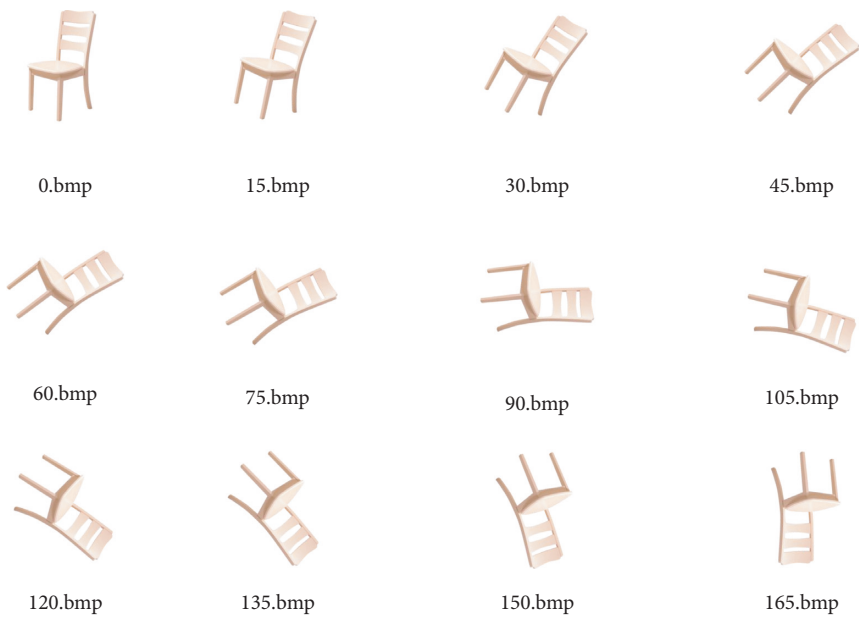

Figure 5: Images after rotation.

Table 3: Rotation test.

Rotation angle	0	15	30	45	60	75	90	105	120	135	150	165
Difference	0	0.171	0.124	0.0200	0.0135	0.0109	0.0028	0.019	0.028	0.0147	0.0081	0.0192

And, when $1 \neq j$, ε_i, and ε_j are uncorrelated, the joint distribution is $f(x, y)$, and the marginal distribution of X is $f(x)$. In general, $m(x)$ can be considered as the conditional expectation of Y when $X = x$, that is,

$$m(x) = E(Y \mid X = x) = \int y f(y \mid x) \mathrm{d}y = \frac{\int y f(x, y) \mathrm{d}y}{f(x)}. \quad (3)$$

Use the following formula to estimate $m(x)$:

$$\widehat{m}(x) = \frac{\left[1/nh \sum_{i=1}^{n} K(x - x_i/h) y_i\right]}{1/nh \sum_{i=1}^{n} K(x - x_i/h)}. \quad (4)$$

Function K (●) is called kernel, which is actually a weighted average function in essence. The density function $f(x)$ is estimated as follows:

$$\widehat{f}(x) = \frac{1}{nh} \sum_{i=1}^{n} K\left(\frac{x - x_i}{h}\right). \quad (5)$$

Among them, h is called bandwidth, and the size depends on the data. We call this as method of estimating m(x) kernel estimation. The regression model is called kernel regression.

When applied to image interpolation, y_i can be regarded as the gray value of the sampling point, x_i is the sampling point, $m(x)$ is the image gray value function to be obtained, expressed by $Z(x)$, ε_i is the error, and N is the number of samples. At this time, the kernel regression model can be written as follows:

$$\widehat{z}(x) = \frac{\sum_{i=1}^{n} K_h(x - x_i) y_i}{\sum_{i=1}^{n} K_h(x - x_i)}, \quad (6)$$

$$K_h(t) = \frac{1}{h} K\left(\frac{t}{h}\right). \quad (7)$$

From (7), it can be seen that the kernel function actually plays a role of weighted average. In image interpolation, the core idea of the interpolation method is how to select the kernel. Many interpolation methods can be regarded as kernel regression model. The kernel functions of some interpolation methods are given.

The kernel function of the nearest interpolation is as follows:

$$K(x) = \begin{cases} 1, & 0 \leq |x| < 0.5, \\ 0, & 0.5 \leq |x|. \end{cases} \quad (8)$$

The kernel function of the bilinear interpolation method is as follows:

$$K(x) = \begin{cases} 1 - |x|, & 0 \leq |x| < 0.5, \\ 0, & 0.5 \leq |x|. \end{cases} \quad (9)$$

The kernel function of cubic convolution interpolation is as follows:

$$K(x) = \begin{cases} (a+2)|x|^3 - (a+3)|x|^2 + 1, & 0 \leq |x| < 1, \\ a|x|^3 - 5a|x|^2 + 8a|x| - 4a, & 1 \leq |x| < 2, \\ 0, & 2 \leq |x|. \end{cases} \quad (10)$$

The kernel function of B-spline interpolation is as follows:

$$K(x) = \begin{cases} 3|x|^3 - 6|x|^2 + 4, & 0 \leq |x| < 1, \\ -|x|^3 + 6|x|^2 - 12|x| + 8, & 1 \leq |x| < 2, \\ 0, & 2 \leq |x|. \end{cases} \quad (11)$$

It can be seen from (11) that the kernel function is actually the weight, so the kernel function must meet certain conditions [16]. Generally, the kernel function should satisfy the following:

(1) $K(x)$ is nonnegative

(2) $K(x)$ is symmetric

(3) $K(x)$ is unimodal and reaches its maximum at zero, namely,

$$\int_{R^l} tK(x) \mathrm{d}t = 0, \quad \int_{R^l} t^2 K(x) \mathrm{d}t = c. \quad (12)$$

C is a constant.

There are many kinds of kernel functions that meet the above conditions; at present, there are four types of kernel functions that are most used.

(1) Linear kernel function:

$$K(x, x_t) = x \times x_t. \quad (13)$$

(2) Polynomial kernel function:

$$K(x, x_t) = \left[(x \times x_t) + 1\right]^q. \quad (14)$$

(3) Gaussian kernel function:

$$K(x, x_t) = \exp\left[-\frac{\|x - x_t\|^2}{2\sigma^2}\right]. \quad (15)$$

(4) Sigmoid kernel function:

$$K(x, x_t) = \tanh\left(v(x, x_t) + c\right). \quad (16)$$

Gaussian kernel function is widely used because of its separability and locality. The kernel function used in this paper is Gaussian kernel function.

3.4. Rough Feature Matching Based on Gaussian Kernel Function. A scale transformation invariant is proposed to correct the wrong matching problem caused by Euclidean distance, and this method is used to make a rough matching between the image to be matched and the image in the database, which is called rough matching, to obtain a group of candidate images. The specific method is shown as follows.

Assuming that the image signature of an image extracted by the word bag model is $x = (x_1, \ldots, x_k)$, we assume that the image signature after taking photos becomes

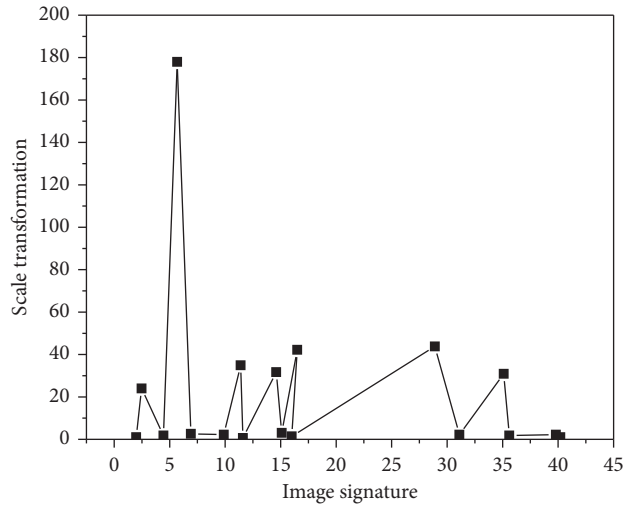

Figure 6: Direct relationship between image signature before taking photos.

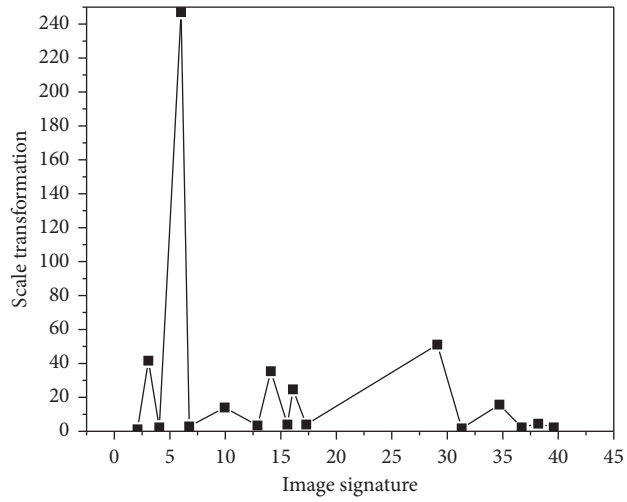

Figure 7: Direct relationship between image signature after taking photos.

$x' = (x'_1, \ldots, x'_k)$; the relative relationship between the image signature before and after taking photos is unchanged; that is, when the number of one feature before taking photos is more than that of another feature, it is still the same after taking photos. As shown in Figures 6 and 7, there is a linear relationship between the image signatures before and after photographing, and this relationship is caused by scale transformation.

We define the linear relationship of image signature before and after photographing as $x' = ax$, where a is the coefficient representing the linear relationship between x' and x. We define an invariant coefficient F, as shown in the following formula:

$$\sigma = \sum_{i=1}^{k} \frac{\sqrt{(x_i - \overline{x})^2}}{\overline{x}}. \tag{17}$$

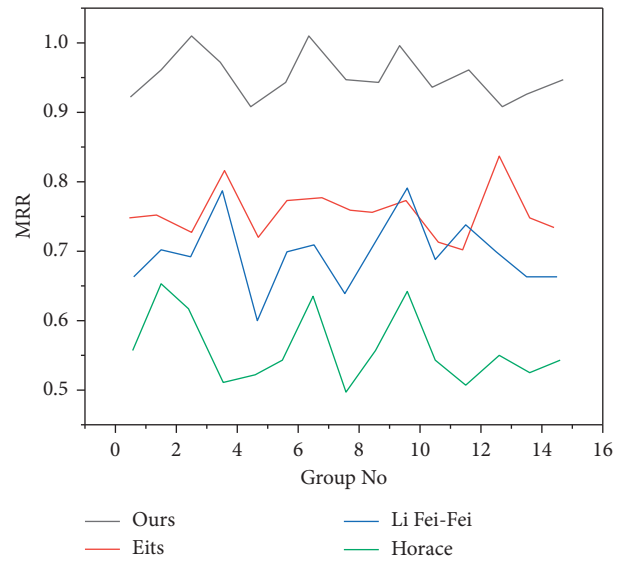

Figure 8: Comparison of MRR results.

Let the invariant coefficient of the image after photographing be σ', and formula (18) proves that the invariant coefficient is fixed before and after photographing.

$$\begin{aligned} \sigma' &= \sum_{i=1}^{k} \frac{\sqrt{(x'_i - \overline{x}')^2}}{\overline{x}'}, \\ &= \sum_{i=1}^{k} \frac{\sqrt{(ax_i - a\overline{x})^2}}{a\overline{x}}, \\ &= \sum_{i=1}^{k} \frac{\sqrt{(x_i - \overline{x})^2}}{\overline{x}}, \\ &= \sigma. \end{aligned} \tag{18}$$

$\sigma' = \sigma$ proves that there is an invariant between the images before and after taking pictures. We use this invariant to correct the error caused by Euclidean distance matching. When the image to be matched is matched with the image in the database by Euclidean distance, a group of similar candidate images will be generated, including both correct and wrong results [17].

4. Experimental Results and Analysis

In order to test the effectiveness of the algorithm in this chapter, we collected thousands of home images as our test database. Then, process the database, extract the visual dictionary, calculate the visual signature of each image, and save it for use. The size of the visual dictionary we use is 180 dimensions, so each visual signature saved in the database is a 180-dimensional histogram.

In order to evaluate the effectiveness of our algorithm, we use the short name of mean reciprocal rank (MRR) to evaluate the algorithm of Gaussian kernel function; as a mechanism to evaluate the advantages and disadvantages of

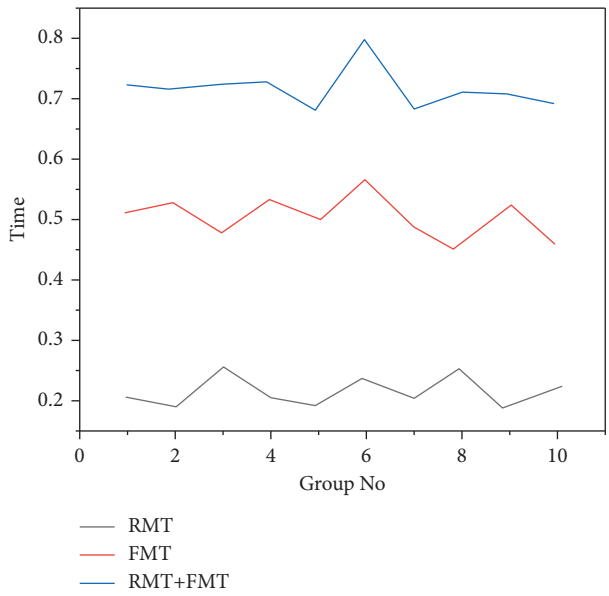

Figure 9: Time consumed by our algorithm.

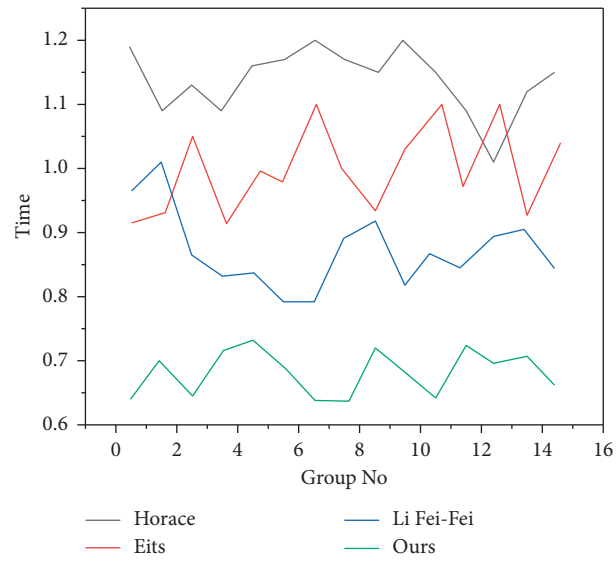

Figure 10: Time performance comparison.

ambiguous algorithms, MRR has certain universality in the world. It mainly measures whether the original image corresponding to the image to be matched in the database is blurred and arranged in front [18]. For a group of Q to be queried, the reciprocal formula of average sorting is as follows:

$$\mathrm{MRR} = \frac{1}{|Q|}\sum_{i=1}^{|Q|}\frac{1}{\mathrm{rank}_i}. \tag{19}$$

The following example illustrates MRR. Suppose we have a fuzzy algorithm, which has been used for three queries to obtain the furniture with the corresponding color. For each query, three furniture are returned as results, the first of which is the best matching result considered by the algorithm. Through these three queries, we can calculate the MRR value of this algorithm: $(1/3 + 1/2 + 1)/3 = 11/18$, which is 0.61.

In order to test and verify the effectiveness of our algorithm, we carried out simulation experiments with a computer with 2.8GhZ CPU and 4G memory, and we did 15 groups of experiments, each containing 100 query images. For each group of experiments, we calculated the MRR value. Figure 8 shows the comparison results of our algorithm with the algorithms of Eits, Horace, and Li Fei Fei. It can be seen from the figure that our algorithm combining coarse matching and fine matching has the best accuracy [19–21].

The time consumed by our algorithm includes two parts: the rough matching time (RMT) and the fine matching time (FMT). As shown in Figure 9, the coarse matching time is the time spent matching a query image with thousands of images in the database, and the fine matching time is the time spent matching a query image with eight candidate images with orb. The total query time is about 0.7 seconds, while it takes about 500 seconds to match thousands of images only with the orb algorithm. In general, we combine coarse matching and fine matching, which can balance the accuracy and speed well. Figure 10 shows the results of comparing the time performance of our algorithm with other algorithms. From the table, we can see that our algorithm has the best time performance [22–24].

5. Conclusion

This article improves the properties of Gabor. There are three main improvements. First, the image filter as a whole is modified by filtering only small local blocks around the feature points, which effectively reduces the filter area and improves the filtering speed. Second, the filter object is changed from the original inner line to gray feature grade mapping enriched the filter information, and third a local coordinate system is introduced to improve the nonreverse rotation characteristics of Gabor. Scale invariance is proposed to update the appropriate results of the structural tensor core regression nonuniform interpolation algorithm, which effectively improves the matching accuracy. Experiments have shown that our algorithm can accurately and quickly capture camera images from blurred images, making it an ideal program for extracting image features.

Data Availability

No data were used to support this study.

Conflicts of Interest

The author declares that there are no conflicts of interest with any financial organizations regarding the material reported in this manuscript.

References

[1] G. Ma, Q. Meng, L. Li, and Y. Ming, "Gradient ratio function of gravity and magnetic data for geological body depth calculation," *Shiyou Diqiu Wuli Kantan/Oil Geophysical Prospecting*, vol. 54, no. 1, pp. 229–234, 2019.

[2] J. Mishra, N. Srivastava, and S. C. Dash, "Comparison of autonomic function using valsalva ratio and 30:15 ratio in chronic renal failure before and after dialysis," *Journal of the Indian Medical Association*, vol. 105, no. 3, pp. 82-83, 2020.

[3] S. Ashbrook, "Architectural photography composition, capture, and digital image processing. (brief article)(book review)," *Procedia Computer Science*, vol. 67, no. 4, pp. 443–470, 2015.

[4] J. M. Davidson, K. Sefiane, and T. Wood, "Fast diffusion reaction in the composition and morphology of coprecipitated carbonates and nitrates of copper (ii), magnesium (ii), and zinc (ii)," *Industrial & Engineering Chemistry Research*, vol. 54, no. 5, pp. 1555–1563, 2015.

[5] E. Cléro, L. Vaillant, N. Hamada, W. Zhang, D. Preston, and D. N. Laurier, "History of radiation detriment and its calculation methodology used in icrp publication 103," *Journal of Radiological Protection*, vol. 39, no. 3, pp. R19–R36, 2019.

[6] J. Reichardt, S. Reichardt, C. A. Hostetler et al., "Mother-of-pearl cloud particle size and composition from aircraft-based photography of coloration and lidar measurements," *Applied Optics*, vol. 54, no. 4, p. B140, 2015.

[7] M. Shavkat, "Calculation of the generalized estimations in sets of features and their interpretation," *International Journal of Software Engineering and its Applications*, vol. 12, no. 3, pp. 29–38, 2018.

[8] L. Hong, R. C. Zhu, G. P. Miao, and G. X. Dong, "Calculation and analysis of added resistance of ships in waves by 3d radiation energy method," *Chuan Bo Li Xue/Journal of Ship Mechanics*, vol. 22, no. 7, pp. 807–817, 2018.

[9] X. Jin, B. Xu, M. Zhou, K. H. Wu, and J. J. Zhao, "Calculation of magnetic entropy changes of la1.2-xtbxsr1.8mn2o7 (x = 0, 0.05) by fitting magnetization function," *Chinese Rare Earths*, vol. 38, no. 3, pp. 98–102, 2017.

[10] X. Liang, P. Chen, B. Liu, and Q. I. Juncheng, "A digital refocusing algorithm based on light field photography," *Nuclear Electronics & Detection Technology*, vol. 35, no. 5, pp. 434–438, 2015.

[11] J.-y. Song, W.-l. Song, J.-p. Huang, and L.-k. Zhu, "Segmentation and focus-point location based on boundary analysis in forest canopy hemispherical photography," *Frontiers of Information Technology & Electronic Engineering*, vol. 17, no. 8, pp. 741–749, 2016.

[12] R. Mark and E. Billo, "Low altitude unmanned aerial photography to assist in rock art studies," *Journal of Electronics and Information Technology*, vol. 35, no. 12, pp. 3030–3036, 2015.

[13] Q.-h. Dai, "Special feature on computational photography," *Frontiers of Information Technology & Electronic Engineering*, vol. 18, no. 9, pp. 1205-1206, 2017.

[14] M. Kim and Jung, "The study of design change in interactive storytelling news based on digital journalism," *journal of the korean society design culture*, vol. 22, no. 4, pp. 11–24, 2016.

[15] W. N. Wang, J. C. Liu, X. M. Xu, Y. Z. Jiang, and L. Wang, "Aesthetic enhancement of images based on photography composition guidelines," *Journal of South China University of Technology*, vol. 43, no. 5, pp. 51–58, 2015.

[16] D. Li, L. Li, P. Li, Y. Li, X. Chen, and J. Huang, "Apoptosis of HeLa cells induced by a new targeting photosensitizer-based PDT via a mitochondrial pathway and ER stress," *OncoTargets and Therapy*, vol. 8, no. 2, pp. 703–711, 2015.

[17] I. Echizen and T. Ogane, "Biometricjammer: method to prevent acquisition of biometric information by surreptitious photography on fingerprints," *IEICE - Transactions on Info and Systems*, vol. E101.D, no. 1, pp. 2–12, 2018.

[18] T. T. Khaing, T. Ruennark, P. Aimmanee, S. Makhanov, and N. Kanchanaranya, "Glaucoma detection in mobile phone retinal images based on adi-gvf segmentation with em initialization," *ECTI Transactions on Computer and Information Technology (ECTI-CIT)*, vol. 15, no. 1, pp. 134–149, 2021.

[19] A. I. Pavlova, V. K. Kalichkin, and A. V. Kalichkin, "Creation of the digital elevation model with the use of unmanned aerial vehicle," *Siberian Herald of Agricultural Science*, vol. 49, no. 3, pp. 70–78, 2019.

[20] Y. Wu, F. Peng, Y. Peng, X. Kong, H. Liang, and Q. Li, "Dynamic 3d simulation of flood risk based on the integration of spatio-temporal gis and hydrodynamic models," *ISPRS International Journal of Geo-Information*, vol. 8, no. 11, p. 520, 2019.

[21] A. Abbas, S. A. Fadhil, Z. A. Jaaz, and A. Ahmed, "Evolution in image steganography; an efficacious route for handling areas of colour noise in digital photography," *Solid State Technology*, vol. 63, no. 6, p. 13, 2020.

[22] H. Singh, "Detail enhanced multi-exposure image fusion based on edge preserving filters," *ELCVIA - Electronic Letters on Computer Vision and Image Analysis*, vol. 16, no. 2, p. 13, 2018.

[23] H. Hassan, A. K. Bashir, R. Abbasi, W. Ahmad, and B. Luo, "Single image defocus estimation by modified Gaussian function," *Transactions on Emerging Telecommunications Technologies*, vol. 30, no. 6, Article ID e3611, 2019.

[24] R. Abbasi, N. M. Faseeh Qureshi, H. Hassan et al., "Generalized PVO-based dynamic block reversible data hiding for secure transmission using firefly algorithm," *Transactions on Emerging Telecommunications Technologies*, vol. 33, no. 3, Article ID e3680, 2022.